

The Real and Redshift Space Density Distribution Function for Large-Scale Structure in the Spherical Collapse Approximation

Robert J. Scherrer¹ and Enrique Gaztañaga^{2,3}

¹*Department of Physics and Department of Astronomy, Ohio State University, Columbus, OH 43210*

²*INAOE, Astrofísica, Tonantzintla, Apdo Postal 216 y 51, Puebla 7200, Mexico*

³*Institut d'Estudis Espacials de Catalunya, Research Unit (CSIC), Edf. Nexus-104-c/Gran Capita 2-4, 08034 Barcelona, Spain*

26 October 2018

ABSTRACT

We use the spherical collapse (SC) approximation to derive expressions for the smoothed redshift-space probability distribution function (PDF), as well as the p -order hierarchical amplitudes S_p , in both real and redshift space. We compare our results with numerical simulations, focusing on the $\Omega = 1$ standard CDM model, where redshift distortions are strongest. We find good agreement between the SC predictions and the numerical PDF in real space even for $\sigma_L \gtrsim 1$, where σ_L is the linearly-evolved rms fluctuation on the smoothing scale. In redshift space, reasonable agreement is possible only for $\sigma_L \lesssim 0.4$. Numerical simulations also yield a simple empirical relation between the real-space PDF and redshift-space PDF: we find that for $\sigma < 1$, the redshift space PDF, $P[\delta_{(z)}]$, is, to a good approximation, a simple rescaling of the real space PDF, $P[\delta]$, i.e., $P[\delta/\sigma] d[\delta/\sigma] = P[\delta_{(z)}/\sigma_{(z)}] d[\delta_{(z)}/\sigma_{(z)}]$, where σ and $\sigma_{(z)}$ are the real-space and redshift-space rms fluctuations, respectively. This result applies well beyond the validity of linear perturbation theory, and it is a good fit for both the standard CDM model and the Λ CDM model. It breaks down for SCDM at $\sigma \approx 1$, but provides a good fit to the Λ CDM models for σ as large as 0.8.

Key words: galaxies: clustering, large-scale structure of universe

1 INTRODUCTION

One of the central statistical quantities of interest in the study of large-scale structure is $P[\rho]$, the one-point probability distribution function (PDF) of the density field ρ . In the linear regime, the PDF simply retains its Gaussian shape, with the variance scaling up as the square of the growth factor. In the nonlinear regime, however, $P[\rho]$ diverges away from its (presumably Gaussian) initial shape.

A number of recent studies have been undertaken to predict analytically the evolution of the PDF. Kofman et al. (1994) calculated the PDF produced by the Zeldovich approximation. Given a formalism to calculate the cumulants of the evolved distribution (Peebles 1980; Fry 1984; Bernardeau 1992a, hereafter B92), the Edgeworth expansion can be employed to derive an approximate expression for the PDF (Juszkiewicz et al. 1995, Bernardeau & Kofman 1995). A better alternative is to derive a similar expansion around the Gamma PDF (Gaztañaga, Fosalba & Elizalde 2000). Unlike the Edgeworth expansion, the Gamma expansion always yields positive densities. The generating function for these cumulants can be used to derive the Fourier transform of

the PDF, which can be inverted to give the PDF in the form of an integral (Bernardeau 1994). Alternatively, this generating function can be transformed into a local Lagrangian mapping which, when applied to the initial Gaussian density field, gives a PDF with the desired tree-level hierarchical amplitudes (Protogeros & Scherrer 1997, hereafter PS; Protogeros, Melott, & Scherrer 1997). Fosalba and Gaztañaga (1998a, hereafter FG) showed that when shear is neglected, the equations of motion automatically produce a local Lagrangian mapping which exactly reproduces the tree-level hierarchical amplitudes (also Fosalba and Gaztañaga 1998b, Gaztañaga & Fosalba 1998). It is this approach, neglecting shear in the cosmological equations of motion, which we will utilize here. Fosalba & Gaztañaga dubbed their approximation the “spherical collapse” (SC) approximation; although we adopt their terminology, it would perhaps be more accurate to refer to this approximation as “shear-free collapse”. The SC model has also been used to model the PDF of QSO Ly- α absorbers (Gaztañaga & Croft 1999).

Of course, the three-dimensional distribution of galaxies is observed in redshift space rather than real space, with the radial coordinate distorted by the peculiar velocities of

arXiv:astro-ph/0105534v2 25 Jul 2001

the galaxies. Hence, the most physically relevant quantity is not the PDF in real space, but the redshift-space PDF. While the evolution of the hierarchical amplitudes in redshift space has been examined in some detail (Bouchet et al. 1995; Hivon et al. 1995; Scoccimarro et al. 1999), comparatively less work has been done on the distortion of the full PDF in redshift space. Kaiser (1987) showed that, to lowest order, the rms fluctuation in redshift space, $\sigma_{(z)}$, is related to the real-space rms fluctuation σ , via

$$\sigma_{(z)}^2 = \left[1 + \frac{2}{3}f_\Omega + \frac{1}{5}f_\Omega^2 \right] \sigma^2 \quad (1)$$

where $f_\Omega \sim \Omega^{0.6}$. (Eq. 1 assumes that the bias parameter is unity. We make this assumption throughout, although bias can be incorporated into our formalism if the form of the bias is prescribed). The effect of redshift distortions on the skewness was calculated by Bouchet et al. (1995) and Hivon et al. (1995). They found that redshift distortions have little effect on the skewness. For $\Omega = 1$, for instance, the redshift-space skewness is well-approximated by (Hivon et al. 1995) $S_{3(z)} = 35.2/7 - 1.15(n+3)$; this compares with a real-space result of $S_3 = 34/7 - (n+3)$. (This theoretical result for the redshift-space skewness does not agree with numerical simulations except at very large length scales; see, e.g., Fig. 3 below). A systematic method to calculate the higher-order perturbation theory kernels in redshift space has been given by Scoccimarro, Couchman, & Frieman (1999). The most detailed treatments thus far have been given by Hui, Kofman, and Shandarin (2000), who calculated the redshift-space PDF in the context of the Zeldovich approximation, and by Watts and Taylor (2000) who calculated the redshift-space PDF in second-order perturbation theory.

In the next section, we derive the local Lagrangian mapping corresponding to the SC model, and apply it to Gaussian initial conditions to derive the real-space density distribution function. In Section 3, we derive an approximation to the redshift distortion of the density field based on the SC approximation. We calculate the corresponding redshift-space hierarchical moments and the redshift-space PDF in the SC approximation and compare the PDF to numerical simulations in redshift space. We also derive an interesting empirical relation between the real-space PDF and the redshift-space PDF. Our conclusions are summarized in Section 4.

2 THE PDF IN THE SC MODEL

2.1 Theory of the SC PDF

One class of approximations to the evolution of large scale structure are local Lagrangian mappings, in which the density at a Lagrangian point \mathbf{q} at a time t is taken to be a function only of t and the initial value of the density at \mathbf{q} ,

$$\eta(\mathbf{q}, t) = N(t)f[\delta_L(\mathbf{q})], \quad (2)$$

where $\eta = \rho/\bar{\rho}$, with $\bar{\rho}$ the mean density, and δ_L is the linearly-evolved initial density fluctuation ($\delta_L = \eta_L - 1$):

$$\delta_L(t) = D(t)\delta(t_0). \quad (3)$$

In equation (2), $N(t)$ is a normalizing factor chosen so that $\int P[\eta]d\eta = 1$:

$$N(t) = \left\langle \frac{1}{f(\delta_L)} \right\rangle. \quad (4)$$

A stochastic field of density fluctuations $\delta(\mathbf{x})$ can be described in terms of its cumulants κ_p , which are given by $\kappa_2 \equiv \sigma^2 = \langle \delta^2 \rangle$, $\kappa_3 = \langle \delta^3 \rangle$, $\kappa_4 = \langle \delta^4 \rangle - \langle \delta^2 \rangle^2 \dots$. An initially Gaussian density field evolving gravitationally has the property that $\kappa_p/\sigma^{2(p-1)}$ goes to a constant in the limit where σ goes to zero, where σ is the rms density fluctuation (Peebles 1980, Fry 1984, Bernardeau 1992). Hence, it is conventional to define the hierarchical amplitudes S_p given by:

$$S_p(\sigma) \equiv \frac{\kappa_p}{(\sigma^2)^{p-1}} \quad (5)$$

The values of S_p in the limit where $\sigma \rightarrow 0$ are called the tree-level hierarchical amplitudes.

This formalism can be exploited to derive an approximation to the PDF in the quasi-linear regime. For small fluctuations, a generic local Lagrangian mapping can be expressed in a Taylor series:

$$\eta(\mathbf{q}) = f[\delta_L(\mathbf{q})] = \sum_k \frac{\nu_k}{k!} \delta_L^k(\mathbf{q}) \quad (6)$$

It can be shown (PS, FG) that for the local Lagrangian mapping given in equation (2), expanded as a Taylor series as in equation (6), the hierarchical amplitudes are given by

$$S_3(0) = 3\nu_2, \quad (7)$$

$$S_4(0) = 4\nu_3 + 12\nu_2^2, \quad (8)$$

and so on. These amplitudes can be made identical to those of exact tree-level perturbation theory if we take the mapping in Eq. (6) to be given by (B92, FG):

$$\begin{aligned} \eta &= N \frac{9}{2} \frac{(\theta - \sin \theta)^2}{(1 - \cos \theta)^3}, \\ \delta_L &= \frac{3}{5} \left[\frac{3}{4} (\theta - \sin \theta) \right]^{2/3}, \end{aligned} \quad (9)$$

for $\delta_L > 0$, $\eta > 1$, and

$$\begin{aligned} \eta &= N \frac{9}{2} \frac{(\sinh \theta - \theta)^2}{(\cosh \theta - 1)^3}, \\ \delta_L &= -\frac{3}{5} \left[\frac{3}{4} (\sinh \theta - \theta) \right]^{2/3}, \end{aligned} \quad (10)$$

for $\delta_L < 0$, $\eta < 1$. [In this paper, we assume Gaussian initial conditions, but this result can be extended to non-Gaussian initial conditions as well (Gaztañaga & Fosalba 1998)].

There is a physical basis for this result: in the limit where shear is neglected, the equations of perturbation growth become (FG)

$$\ddot{\delta} + \frac{\dot{a}}{a} \dot{\delta} - \frac{4}{3} \frac{\dot{\delta}^2}{(1+\delta)} = 4\pi G a^2 \delta(1+\delta), \quad (11)$$

where the dot denotes the convective derivative with respect to conformal time. (Hence, equation (11) is an equation for the Lagrangian density). But equation (11) is identical to the equation for δ in spherical collapse, so the solution is the local Lagrangian SC mapping given by Eqs. (9)-(10). Furthermore, the Fourier-space integrals which give the tree-level hierarchical amplitudes are spherically symmetric, guaranteeing that the SC approximation gives the correct hierarchical amplitudes at tree level (FG). Although this approximation was dubbed the ‘‘spherical-collapse approximation’’

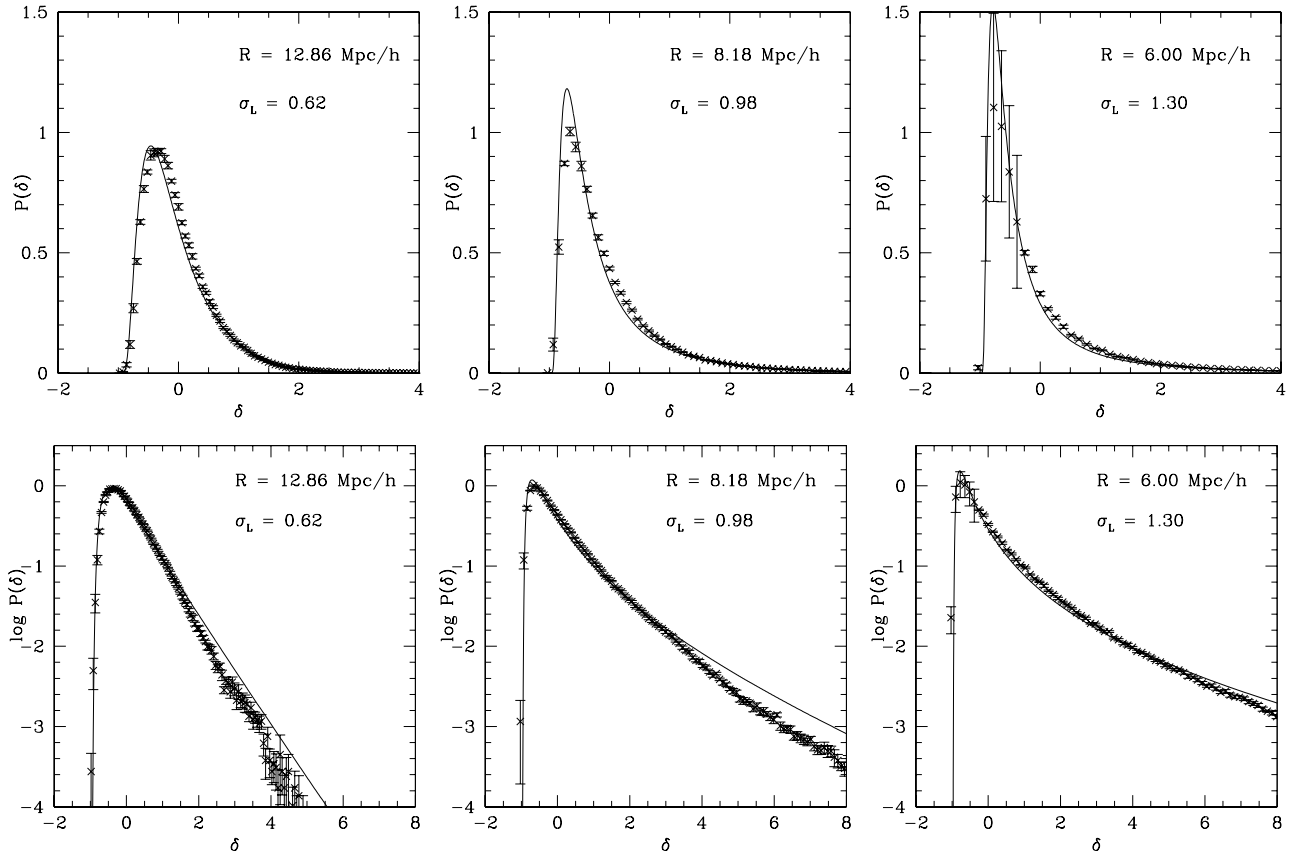


Figure 1. The PDF $P[\delta]$ (top) and $\log P[\delta]$ (bottom) as a function of δ in the SCDM model. Points with $1 - \sigma$ error bars are from the numerical simulation. Solid curve is the SC theoretical prediction. Each pair of panels corresponds to a different smoothing scale R and therefore a different linear rms fluctuation σ_L , indicated in the figure.

(FG), it does not presume or imply that the actual physical collapse is spherically symmetric; rather, it proceeds from the approximation that the clustering is shear-free. This approximation should not be confused with the well-known analytic results for actual spherical collapse (Peebles 1980).

For the SC approximation we have:

$$\begin{aligned}
 \nu_2 &= \frac{34}{21} \sim 1.62, \\
 \nu_3 &= \frac{682}{189} \sim 3.61, \\
 \nu_4 &= \frac{446440}{43659} \sim 10.22, \\
 \nu_5 &= \frac{8546480}{243243} \sim 35.13,
 \end{aligned} \tag{12}$$

and note that $\nu_1 = 1$ to produce the linear theory result. As noted, these numbers give the correct contribution to the p th-order cumulants, κ_p , for Gaussian initial conditions, e.g., $S_3 = 34/7$ (Peebles 1980, Section 42).

We now derive the PDF in the SC approximation. The SC local Lagrangian mapping which relates $\delta_L(\mathbf{q})$ to $\eta(\mathbf{q})$ is given by Eqs. (9) and (10). In our discussions below, the mapping $\eta = Nf(\delta_L)$ is always understood to refer to equations (9) and (10), although one cannot write down a non-parametric form for $f(\delta_L)$. These equations also define an inverse function: $\delta_L = f^{-1}(\eta/N)$; it is $\delta_L(\eta/N)$ as defined by equations (9) and (10) which actually enters into our

equations for the PDF. The evolved PDF (given, as usual, in Eulerian space) is (PS)

$$P[\eta] = P_0[\delta_L(\eta/N)] \frac{1}{\eta} \frac{d\delta_L(\eta/N)}{d\eta} \tag{13}$$

where P_0 is the initial (unevolved) density distribution function. The normalizing factor N is most easily derived from:

$$N = \int_0^\infty P_0(\delta_L(x)) \frac{1}{x} \frac{d\delta_L(x)}{dx} dx, \tag{14}$$

where we have used the change of variables $x = \eta/N$. For Gaussian initial conditions, P_0 is a Gaussian, and we get

$$P[\eta] = \frac{1}{\sqrt{2\pi}\sigma_L} \exp\left[-\frac{\delta_L(\eta/N)^2}{2\sigma_L^2}\right] \frac{1}{\eta} \frac{d\delta_L(\eta/N)}{d\eta} \tag{15}$$

where σ_L is the linearly evolved rms fluctuation:

$$\sigma_L(t) = D(t)\sigma_0, \tag{16}$$

and N is given by

$$N = \int_0^\infty \frac{1}{\sqrt{2\pi}\sigma_L} \exp\left[-\frac{\delta_L(x)^2}{2\sigma_L^2}\right] \frac{1}{x} \frac{d\delta_L(x)}{dx} dx. \tag{17}$$

This expression gives the PDF for an unsmoothed density field, which is not physically observable. If we smooth the final density field with a spherical top-hat window function, then we obtain a new ‘‘smoothed’’ local Lagrangian mapping density $f_S(\delta_L)$, which is given in terms

of the unsmoothed mapping f through the implicit relation (Bernardeau 1994; PS; FG):

$$f_S(\delta_L) = f\left(\delta_L \frac{\sigma(f_S(\delta_L)R_0)}{\sigma(R_0)}\right) \quad (18)$$

where R_0 is the radius of the spherical top-hat, and $\sigma(R_0)$ is the rms fluctuation of the linear density field (in practice, derived by integrating over the linear power spectrum). Taking $\eta_S = N f_S(\delta_L)$, where N is the new (smoothed) normalization factor, this expression can be recast in the form

$$\delta_L(\eta_S/N) = f^{-1}(\eta_S/N) \frac{\sigma(R_0)}{\sigma(R_0 \eta_S/N)}. \quad (19)$$

If the linear power spectrum is a power law, $P(k) \propto k^n$, equations (18) and (19) simplify to (Bernardeau 1994)

$$f_S(\delta_L) = f\left[\delta_L f_S(\delta_L)^{-(n+3)/6}\right], \quad (20)$$

which gives

$$\delta_L(\eta_S/N) = f^{-1}(\eta_S/N) [\eta_S/N]^{(n+3)/6} \quad (21)$$

The expression for δ_L from either equation (19) or equation (21) can be substituted into equations (15)-(17) to obtain $P_S(\eta)$ (the PDF of the smoothed density field).

2.2 Test with Nbody simulations

To test our approximations for the PDF, we compare to a set of 10 standard cold dark matter (SCDM) simulations with 64^3 particles over an $L = 180$ Mpc/ h box. (We also used simulations with an $L \simeq 400$ Mpc/ h box to test for volume effects. See Baugh, Gaztañaga & Efstathiou 1995, for more details on these simulations). By smoothing over different lengths we derived a set of PDF's for different values of the linear rms fluctuation σ_L .

The results are displayed in Fig. 1. It is clear that the SC approximation provides excellent agreement with the numerical PDF even for $\sigma_L \gtrsim 1$, except for the large- δ tail of the distribution. These results are consistent with those of Protogeros, Melott, & Scherrer (1997), who used a less-accurate Lagrangian mapping which mimics the SC approximation and found good agreement with the PDF for power-law initial conditions.

3 THE REDSHIFT DISTORTION OF THE PDF

3.1 Preliminaries

A particle at a position \mathbf{r} in real space, with local velocity \mathbf{v} , will be measured to lie at a position $\mathbf{r}_{(z)}$ in redshift space, given by:

$$\mathbf{r}_{(z)} = \mathbf{r} + (v_r/H)\hat{\mathbf{r}} \quad (22)$$

where H is the Hubble parameter, and $\hat{\mathbf{r}}$ points radially outward from the observer. For simplicity, we use the ‘‘infinite observer’’ approximation, so that the redshift direction is taken to lie parallel to one of the Cartesian axes, which we take to be the x axis. Then we have:

$$\mathbf{r}_{(z)} = \mathbf{r} + (v_x/H)\hat{\mathbf{x}}. \quad (23)$$

It is convenient to make the substitution $\mathbf{u} = \mathbf{v}/H$, so that

$$\mathbf{r}_{(z)} = \mathbf{r} + u_x \hat{\mathbf{x}}. \quad (24)$$

From mass conservation, we obtain the relation between $\eta_{(z)}$, the value of η measured at a particular point in redshift space, and the corresponding η at the same (Lagrangian) point in real space, where we can treat the redshift-space distortion as a Lagrangian mapping:

$$\eta_{(z)} = \frac{\eta}{1 + (du_x/dx)}, \quad (25)$$

(see also Hui et al. 2000). Equation (25) is exact (for the infinite-observer case) and can be used, in principle, to calculate the redshift-distortion of the PDF. Such a calculation can be carried out for the skewness (Bouchet et al. 1995; Hivon et al. 1995; Scoccimarro et al. 1999), but there is no simple way to apply it to the full PDF.

Hence, we make an approximation which is appropriate to the SC model. First we take du_x/dx to be given by

$$\frac{du_x}{dx} = \frac{1}{3}\theta, \quad (26)$$

where $\theta \equiv \nabla \cdot \mathbf{u}$. This relation between du_x/dx and θ is what would be expected in the limit where shear (and vorticity) are neglected, and our approximation has the advantage that the statistical properties of θ are well-known in tree-level perturbation theory. We get

$$\eta_{(z)} = \frac{\eta}{1 + (1/3)\theta} \quad (27)$$

which gives, for δ ,

$$\delta_{(z)} = \frac{\delta - (1/3)\theta}{1 + (1/3)\theta} \quad (28)$$

We can use the continuity equation:

$$\frac{d\eta}{dt} + H\eta\theta = 0, \quad (29)$$

to express θ as a Lagrangian mapping of δ_L :

$$\theta = -\frac{1}{H\eta} \frac{d\eta}{dt} = -f_\Omega \frac{\delta_L}{\eta} \frac{d\eta}{d\delta_L}, \quad (30)$$

where $f_\Omega \equiv d \ln D / d \ln a$, comes from applying the chain rule to the derivative of the linear growth factor: $\delta_L = D(t)\delta_0$.

3.2 Hierarchical moments

Consider first the case of an unsmoothed density field. For small fluctuations all we need are the coefficients of the corresponding Taylor expansion:

$$\eta_{(z)} = \sum_k \frac{\nu_k(z)}{k!} \delta_L^k. \quad (31)$$

We find for the first few orders:

$$\begin{aligned} \nu_{1(z)} &= 1 + \epsilon \\ \nu_{2(z)} &= \nu_2 + 2\epsilon\nu_2 + 2\epsilon^2 \\ \nu_{3(z)} &= \nu_3 + 3\epsilon\nu_3 + 6\epsilon^2(2\nu_2 - 1) + 6\epsilon^3 \\ \nu_{4(z)} &= \nu_4 + 4\epsilon\nu_4 + 24\epsilon^2(\nu_3 + \nu_2^2 - 5\nu_2/2 + 1) \\ &\quad + 24\epsilon^3(3\nu_2 - 2) + \epsilon^4, \end{aligned} \quad (32)$$

where $\epsilon \equiv f_\Omega/3$. Note that in redshift space $\nu_{1(z)} \neq 1$, because of the ‘‘Kaiser’’ effect.

First consider the hierarchical amplitudes. For the redshift variance we have:

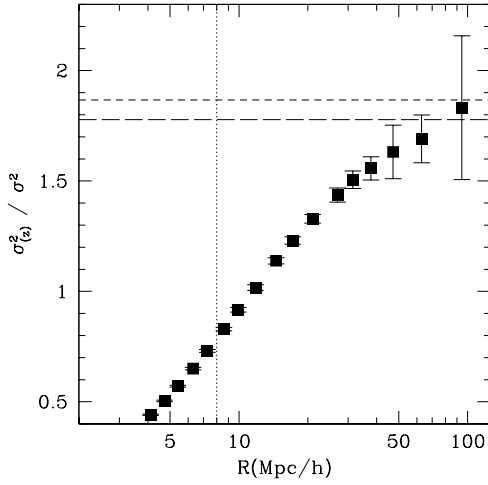


Figure 2. The ratio of the redshift to real space variance $\sigma_{(z)}^2/\sigma^2$ as a function of smoothing scale in SCDM simulations (points with error-bars) as compared to the “Kaiser” results (short-dashed lines) and the linear SC model (long-dashed lines). The dotted vertical line marks the scale where the linear variance is unity, i.e. $\sigma_L = 1$. Error bars are $1 - \sigma$.

$$\sigma_{(z)}^2 = (1 + \epsilon)^2 \sigma_L^2 + \mathcal{O}(\sigma_L^4). \quad (33)$$

Note that this gives a reasonable approximation to the “Kaiser” effect in Eq. (1). For example, for $f_\Omega \rightarrow 1$ ($\epsilon \rightarrow 1/3$), the expression above gives $\sigma_{(z)}^2/\sigma_L^2 = 16/9 \simeq 1.78$, compared with $\sigma_{(z)}^2/\sigma_L^2 = 28/15 \simeq 1.87$ in Eq. (1). These results are compared with (fully non-linear) SCDM simulations in Fig. 2.

For the redshift-space skewness $S_{3(z)}$ and kurtosis $S_{4(z)}$, at leading order, are:

$$\begin{aligned} S_{3(z)} &= \frac{3\nu_{2(z)}}{\nu_{1(z)}^2} = \frac{S_3 + 2\epsilon S_3 + 6\epsilon^2}{(1 + \epsilon)^2} + \mathcal{O}(\sigma_L^2), \quad (34) \\ S_{4(z)} &= \frac{S_4 + 4\epsilon S_4 + 3\epsilon^2(S_4 + 4S_3^2/9 + 32S_3/3 - 8)}{(1 + \epsilon)^4} \\ &+ \frac{48\epsilon^3 S_3 + 72\epsilon^4}{(1 + \epsilon)^4} + \mathcal{O}(\sigma_L^2), \end{aligned}$$

where $S_3 = 3\nu_2$ and $S_4 = 12\nu_2^2 + 4\nu_3$ are the corresponding real-space leading order results. In the limit $f_\Omega \rightarrow 0$ we get the real-space results, as expected. In the limit $f_\Omega \rightarrow 1$ ($\epsilon \rightarrow 1/3$) we have, at leading order:

$$\begin{aligned} S_{3(z)} &= \frac{15}{16} S_3 + \frac{3}{8}, \quad (35) \\ S_{4(z)} &= \frac{27}{32} S_4 + \frac{3}{64} S_3^2 + \frac{27}{16} S_3 - \frac{9}{16}. \end{aligned}$$

So redshift distortions are not very large at leading order even in the case when $f_\Omega \rightarrow 1$. For the skewness, we get $S_{3(z)} = 4.93$, in excellent agreement with the results of exact perturbation theory, which predicts $S_{3(z)} = 5.03$ (Hivon et al. 1995), a difference of roughly 2%. For the kurtosis, we obtain $S_{4(z)} = 47.5$, (no exact calculation of $S_{4(z)}$ has been done thus far), which compares with a real-space value of $S_4 = 45.9$. Like the skewness, the kurtosis is only slightly increased by redshift distortions.

In practice, one needs to reach very large scales ($R \gtrsim 100 h^{-1}\text{Mpc}$) to get to the regime where leading order is a good approximation. This is illustrated in Fig. 2, which shows how the ratio $\sigma_{(z)}^2/\sigma^2$ estimated from SCDM Nbody simulations (presented in Section 2.2), only reaches the linear regime at $R \gtrsim 100 h^{-1}\text{Mpc}$, even when the simulated box is $L = 400 h^{-1}\text{Mpc}$ and the scale of non-linearity is $8 h^{-1}\text{Mpc}$.

We should therefore consider next to leading order corrections. For the variance we have:

$$\begin{aligned} \sigma_{(z)}^2 &= s_{2,2(z)} \sigma_L^2 + s_{2,4(z)} \sigma_L^4, \quad (36) \\ s_{2,2(z)} &= (1 + \epsilon)^2, \\ s_{2,4(z)} &= \frac{8}{3} s_{2,4} + \frac{212S_3^2 + S_3 - 716}{162}. \end{aligned}$$

For the skewness and $f_\Omega \rightarrow 1$:

$$\begin{aligned} S_{3(z)} &= S_{3,0(z)} + S_{3,2(z)} \sigma_L^2, \quad (37) \\ S_{3,0(z)} &= \frac{15}{16} S_{3,0} + \frac{3}{8}, \\ S_{3,2(z)} &= \frac{28}{9} S_{3,2} \\ &+ \frac{3772 - 1608S_3 - 1149S_3^2 - 13S_3^3 + 864S_4}{486}, \end{aligned}$$

where the values on the right-hand side are the ones in real space. We can see from the expressions above that the corrections are quite different in real and redshift space.

Now consider the effects of smoothing. For power-law initial conditions, with a power spectrum $P[k] \propto k^n$, it is possible to show that (Juszkiewicz, Bouchet and Colombi 1993)

$$S_{3S} = S_3 + \gamma, \quad (38)$$

where $\gamma = -(n + 3)$. Bernardeau (1994) has shown that the above result is also true for a generic power spectrum, where $\gamma = \gamma(R) = d \log(\sigma^2)/d \log(R)$. In Section 3.4 below, we will argue that the effects of smoothing on the redshift-distorted PDF are identical to the effects in real space (e.g., Eqs. 50-51). Hence, we expect that

$$S_{3(z)S} = S_{3(z)} + \gamma \quad (39)$$

Substituting these two equations into Eq. (34), we obtain

$$S_{3(z)S} = \frac{S_{3S} + 2\epsilon S_{3S} + 6\epsilon^2 + \gamma\epsilon^2}{(1 + \epsilon)^2}. \quad (40)$$

In the limit where $f_\Omega \rightarrow 1$, this becomes

$$S_{3(z)S} = \frac{15}{16} S_{3S} + \frac{3}{8} + \frac{\gamma}{16}. \quad (41)$$

Since $\gamma/16$ is generally small compared to the other terms in the equation, smoothing has a minimal effect on the relation between the real and redshift space skewness.

Fig. 3 shows a comparison of the leading order contribution to S_3 in redshift (dashed line) and real (solid line) space as a function of smoothing scale R (which enters in the above expressions through $\gamma = \gamma(R)$). As can be seen in the figure, the real space predictions work well for $R \geq 10$, while in redshift space we need to go to larger scales to find a similar agreement with leading order results. (This is similar to what happens for the variance, e.g., see Fig. 2).

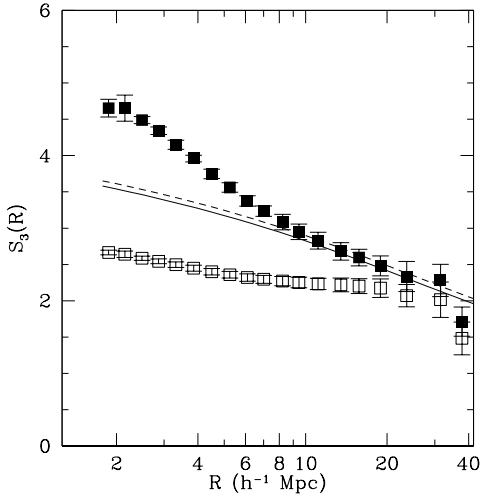


Figure 3. Comparison of the redshift (open squares) and real (closed square) space skewness S_3 , with $1 - \sigma$ error bars, as a function of smoothing scale R , in SCDM simulations. Solid and dashed lines show the leading order SC result in real and redshift space.

3.3 Dimensionless moments

In discussions of large-scale structure, one is usually interested in the hierarchical moments discussed in the previous section. However, as we shall see in Section 3.5 below, we find a simple empirical relationship between $P[\delta]$ and $P[\delta_{(z)}]$. This result can be understood by considering the moments of the normalized field $\mu \equiv \delta/\sigma$. For the variance we have:

$$\sigma_\mu^2 = \langle \mu^2 \rangle_c = 1, \quad (42)$$

in both real and redshift space, by construction. We can define a dimensionless skewness:

$$B_3 \equiv \langle \mu^3 \rangle_c = S_3 \sigma, \quad (43)$$

and in redshift space we find:

$$\begin{aligned} B_{3(z)} &= \frac{S_3 + 2\epsilon S_3 + 6\epsilon^2}{1 + \epsilon} \sigma_L + \mathcal{O}(\sigma_L^3), \\ &= \frac{(1 + 2\epsilon)}{1 + \epsilon} B_3 + \frac{6\epsilon^2}{1 + \epsilon} \sigma_L + \mathcal{O}(\sigma_L^3), \end{aligned} \quad (44)$$

which in the limit $f_\Omega \rightarrow 1$ gives:

$$B_{3(z)} = \frac{5}{4} B_3 + \frac{1}{2} \sigma_L + \mathcal{O}(\sigma_L^3), \quad (45)$$

which should be compared with the leading order real-space result $B_3 = S_3 \sigma_L$. At this order redshift distortions on the skewness are therefore still relatively small, while by definition they are zero in the variance. For the dimensionless kurtosis we find:

$$B_{4(z)} = \frac{3}{2} B_4 + \frac{1}{12} B_3^2 + (3S_3 - 1) \sigma_L^2 + \mathcal{O}(\sigma_L^4) \quad (46)$$

The next to leading order term, $B_{3,3} \sigma_L^3$ is, in the limit $f_\Omega \rightarrow 1$:

$$\begin{aligned} B_{3,3(z)} &\simeq 2.95 - 2.74 S_3 + 4.25 S_3^2 + 4.73 S_3^3 - 1.6 S_4 \\ &- 5.8 S_3 S_4 + 1.24 S_5 \end{aligned} \quad (47)$$

while in real space ($f_\Omega \rightarrow 0$):

$$\begin{aligned} B_{3,3} &= -2 + \frac{3}{2} S_3 + \frac{3}{2} S_3^2 + \frac{121}{108} S_3^3 + \frac{11}{8} S_3 S_4 \\ &- S_4 + \frac{3}{10} S_5 \end{aligned} \quad (48)$$

For the SCDM model at large scales, where $\gamma \simeq -2$, we have: $S_3 \simeq 2.86$, $S_4 \simeq 13.9$ and $S_5 \simeq 97$. We then find $B_{3,3(z)} \simeq 7.4$ while in real space: $B_{3,3} \simeq 1.16$. So there is a significant difference in these higher corrections, although the resulting change in B_3 gets smaller as $\sigma_L \rightarrow 0$.

3.4 The redshift-space PDF

To obtain the final density at a given Lagrangian point, we first apply the SC approximation to obtain η as a function of δ_L in real space and then apply the redshift mapping in equation (27), with θ given by equation (30), to go from η to $\eta_{(z)}$. The combination of these two mappings can be treated as a single local Lagrangian mapping. We obtain, for the local Lagrangian relation between δ_L and the redshift-distorted $\eta_{(z)}$:

$$\eta_{(z)} = F(\delta_L) \equiv \frac{f(\delta_L)}{1 - \frac{1}{3} f_\Omega \frac{\delta_L}{f(\delta_L)} \frac{df(\delta_L)}{d\delta_L}} \quad (49)$$

where the function f is given by equations (9) and (10). Finally, we must include the effects of smoothing. To do this, we apply equation (19) or (21) to the redshift-distorted density field. For a power-law power spectrum, for example we obtain:

$$\delta_L(\eta_{(z)S}/N) = F^{-1}(\eta_{(z)S}/N) (\eta_{(z)S}/N)^{(n+3)/6}, \quad (50)$$

while in the general case, we get

$$\delta_L(\eta_{(z)S}/N) = F^{-1}(\eta_{(z)S}/N) \frac{\sigma(R_0)}{\sigma(R_0 \eta_{(z)S}/N)}. \quad (51)$$

In these equations, F^{-1} is the inverse of the function F , given in equation (49), which transforms δ_L into $\eta_{(z)}$.

A couple of comments are in order regarding our smoothing methodology: we have convolved the local Lagrangian mappings $\delta_L \rightarrow \eta$ and $\eta \rightarrow \eta_{(z)}$ into a single local Lagrangian mapping $\eta_{(z)} = F(\delta_L)$, given by equation (49); it is this mapping which enters into Bernardeau's smoothing formalism. Note also that we are performing our operations in the correct order: equations (49) and (50) or (51) amount to first evolving the density field, then applying the redshift distortion, and smoothing the final result.

For Gaussian initial conditions, our final expression for the redshift-distorted PDF is then:

$$P[\eta_{(z)S}] = \frac{1}{\sqrt{2\pi}\sigma_L} \exp\left[-\frac{\delta_L^2}{2\sigma_L^2}\right] \frac{1}{\eta_{(z)S}} \frac{d\delta_L}{d\eta_{(z)S}}, \quad (52)$$

where the function $\delta_L = \delta_L(\eta_{(z)S}/N)$ is given by equations (49) and (50) or (51), and N is given by

$$N = \int_0^\infty \frac{1}{\sqrt{2\pi}\sigma_L} \exp\left[-\frac{\delta_L(x)^2}{2\sigma_L^2}\right] \frac{1}{x} \frac{d\delta_L(x)}{dx} dx. \quad (53)$$

We now test this approximation for the redshift-distorted PDF numerically. The numerical simulations (described in Section 2.2) were used to calculate the redshift

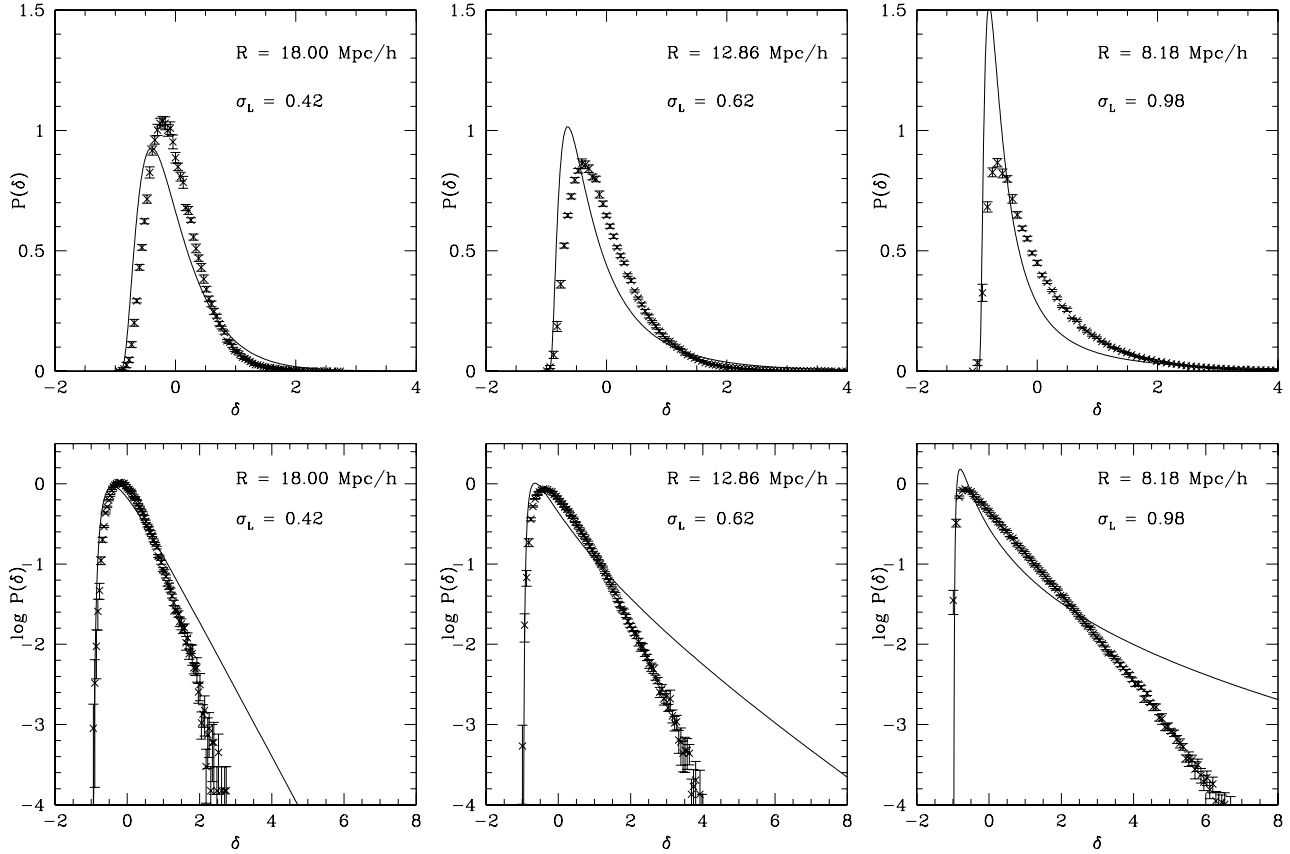


Figure 4. The PDF $P[\delta]$ (top) and $\log P[\delta]$ (bottom) as a function of δ in redshift space. Points with $1 - \sigma$ error bars are from the numerical simulation. Solid curve is the SC theoretical prediction. Each pair of panels corresponds to a different smoothing scale R and therefore a different linear rms fluctuation σ_L , indicated in the figure.

space PDF for a variety of values of σ_L . These are compared with the SC prediction for the redshift-space PDF in Fig. 4.

It is clear that the SC approximation gives a reasonable fit to the redshift-space PDF for $\sigma_L \lesssim 0.4$ but fails for larger values. Despite these problems, the SC approximation appears applicable to larger values of σ_L than does the the Kaiser expression for $\sigma_{(z)}$ (Eq. 1). For example, Eq. (1) predicts $\sigma_{(z)}^2/\sigma^2 = 1.87$. In our numerical simulations, we obtain $\sigma_{(z)}^2/\sigma^2 = 1.21$ for $\sigma_L = 0.42$, corresponding to the left panel in Fig. 4. Thus, Eq. (1) fails badly for σ_L as small as 0.4 (see also Fig. 2), for which the SC approximation provides reasonable agreement with the empirical PDF.

3.5 An interesting empirical result

For $\sigma_L \sim 1$, the SC approximation does a much better job of predicting the real-space PDF than the redshift-space PDF. Hence, we are motivated to consider other possible ways of predicting the latter. Note that when we normalize the distributions to $\mu \equiv \delta/\sigma$, the real and redshift space moments are very similar to leading order. The variances are identical by construction and we have seen that the dimensionless skewness B_3 and kurtosis B_4 are quite similar at leading order. Thus one would expect that when $\sigma_L \rightarrow 0$ the dimensionless redshift PDF would be similar to that in redshift space. Note that $\mu \equiv \delta/\sigma$ and the dimensionless moments

Table 1. The real-space and redshift-space values of the variance, skewness, and kurtosis measured in SCDM simulations for a smoothing scale of $R = 15$ Mpc/h.

	σ	S_3	S_4	B_3	B_4
real	0.482	2.66	11.6	1.28	2.69
z	0.510	2.30	6.8	1.13	1.77

are the natural variables to quantify the amount of non-Gaussian effects on the PDF, as it is evident from the Edgeworth and Gamma expansions (e.g., see Gaztañaga, Fosalba & Elizalde 2000).

In Fig. 5, we provide a comparison of $P[\delta/\sigma]d[\delta/\sigma]$ in real and redshift space. It is obvious from these figures that the agreement is excellent for $\sigma_L \lesssim 0.6$ and only breaks down at $\sigma_L \approx 1$. For $\sigma_L \lesssim 0.6$, the major difference occurs at the large- δ tails of the distributions, indicating that the higher order terms are becoming important. In particular, the real and redshift-space distributions diverge at $\delta/\sigma > 4$.

Note nevertheless that the agreement seems better than one would expect. Consider, for example, the values of the variance, skewness and kurtosis at $R = 15$ Mpc/h given in Table 1. We see that $\sigma_{(z)}^2/\sigma^2$ lies below the linear theory prediction in Eq. (1) (or the SC prediction in Eq. 33), while $S_{3(z)}$ and $S_{4(z)}$ are smaller than the corresponding real space

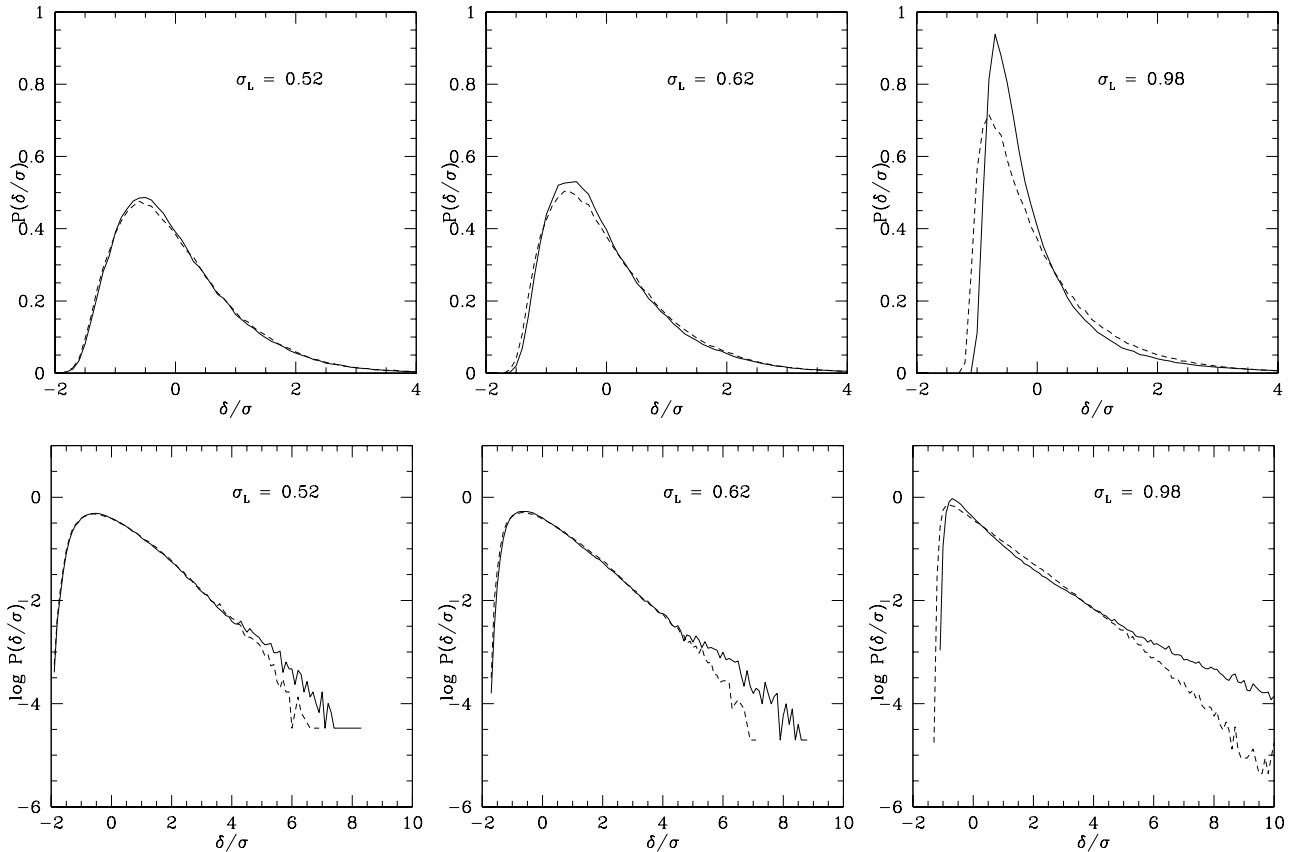


Figure 5. A comparison of the real-space PDF, $P[\delta/\sigma]$ (solid curve) with the redshift-space PDF, $P[\delta_{(z)}/\sigma_{(z)}]$ (dashed curve) in SCDM simulations at the indicated values of σ_L . Error bars have been suppressed for clarity.

values: in the opposite direction to the leading order prediction in Eq. (35). These two effects seem to cancel each other so that the values of the dimensionless skewness B_3 and kurtosis B_4 in real and redshift space are quite similar. This suggests some additional cancellation of the redshift distortions which is not accounted for by the SC model, most likely due to nonlinear effects.

Because of the potential significance of this result, we have repeated this calculation for a flat Λ CDM model with $\Omega_\Lambda = 0.8$ (while this value for Ω_Λ is somewhat larger than that suggested by recent observations, this model and the SCDM model should serve to bracket the likely effect of redshift distortions). Our results are displayed in Fig. 6. Again, we see that, to a good approximation, $P[\delta/\sigma]d(\delta/\sigma)$ is identical in real and redshift space. The agreement here is even better than for the SCDM model; the two distributions are nearly identical for σ as large as 0.8.

4 CONCLUSIONS

The spherical collapse (SC) approximation for the PDF can provide good agreement with both the real-space and redshift-space PDF from numerical SCDM simulations, but it fails at a much smaller value of σ_L in the latter case. In real space, we get good agreement with the numerical results for $\sigma_L \gtrsim 1$, while in redshift space, good agreement can be obtained only for $\sigma_L \lesssim 0.4$. This is most likely due to nonlinear

effects in the redshift-space PDF. An interesting advantage of the SC approach to derive the PDF is the possibility of extending the results to the case of non-Gaussian initial conditions (see also Gaztañaga & Fosalba 1998, Gaztañaga & Croft 1999). We only need to replace P_0 in equation (13) by the corresponding non-Gaussian initial PDF.

We also find an unexpected result in our simulations: the redshift space PDF, $P[\delta_{(z)}]$, is, to a good approximation, a simple rescaling of the real space PDF, $P[\delta]$, i.e., $P[\delta/\sigma]d(\delta/\sigma) = P[\delta_{(z)}/\sigma_{(z)}]d(\delta_{(z)}/\sigma_{(z)})$. This rescaling provides an excellent approximation to the redshift-space PDF for $\sigma_L < 1$ in both the SCDM and Λ CDM models. We have not found an entirely satisfactory explanation for this. While it would be an obvious result from linear theory, its validity extends well beyond the linear regime. For example, this rescaling applies very well to the regime for which $P[\delta]$ is highly non-Gaussian and the Kaiser prediction for $\sigma_{(z)}$ from linear theory (Eq. 1) breaks down. This result seems to stem from a cancellation between the linear effect given by Eq. (25) and the nonlinear redshift distortions. It is perhaps ironic that this simple-minded rescaling gives a much better prediction for the redshift-space PDF than our sophisticated perturbation-theory approximation.

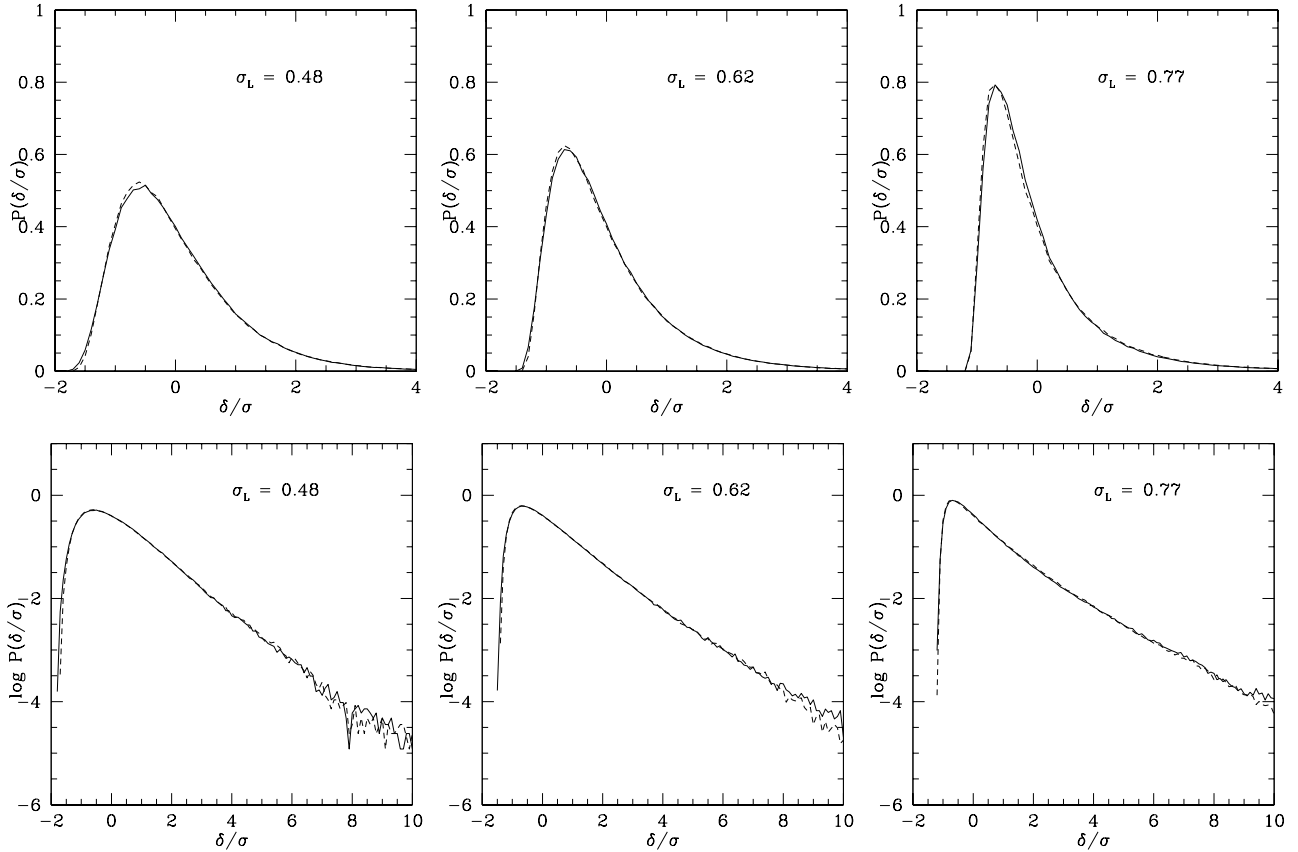


Figure 6. A comparison of the real-space PDF, $P[\delta/\sigma]$ (solid curve) with the redshift-space PDF, $P[\delta(z)/\sigma(z)]$ (dashed curve) in flat Λ CDM simulations at the indicated values of σ_L . Error bars have been suppressed for clarity.

ACKNOWLEDGMENTS

We thank L. Hui, J. Frieman, and R. Scoccimarro for helpful discussions. E.G. acknowledge support by grants from IEEC/CSIC and DGES(MEC)(Spain) project PB96-0925, and Acci3n Especial ESP1998-1803-E. R.J.S. was supported in part by the Department of Energy (DE-FG02-91ER40690). R.J.S. is grateful for the hospitality of the Fermilab Theoretical Astrophysics Group, where this work was initiated.

REFERENCES

- Baugh, C.M., Gaztañaga, E. & Efstathiou, G., 1995 MNRAS, 274, 1049
- Bernardeau, F., 1992a, ApJ, 392, 1 (B92)
- Bernardeau, F., 1992b, ApJ, 390, L61
- Bernardeau, F., 1994, A&A, 291, 697
- Bernardeau, F., Kofman, L., 1995, ApJ 443, 479
- Bouchet, F.R., Colombi, S., Hivon, E., & Juszkiewicz, R., 1995, A&A, 296, 575
- Fosalba, P., & Gaztañaga, E., 1998a, MNRAS, 301, 503 (FG)
- Fosalba, P., & Gaztañaga, E., 1998b, MNRAS, 301, 535
- Fry, J.N., 1984, ApJ, 279, 499
- Gaztañaga, E., & Croft, R.A.C., 1999, MNRAS, 309, 895
- Gaztañaga, E., & Fosalba, P., 1998, MNRAS, 301, 524
- Gaztañaga, E., & Fosalba, E. Elizalde, 2000, ApJ, 539, 522
- Hivon, E., Bouchet, F.R., Colombi, S., & Juszkiewicz, R., 1995, A&A, 298, 643
- Hui, L., Kofman, L., & Shandarin, S.F., 2000, ApJ, 537, 12
- Juszkiewicz, R., Weinberg, D.H., Amsterdamski, P., Chodorowski, M., & Bouchet, F., 1995, ApJ, 442, 39
- Juszkiewicz, R., Bouchet, F. & Colombi, S., 1993, ApJ, 412, L9
- Kaiser, N., 1987, MNRAS, 227, 1
- Kofman, L., Bertschinger, E., Gelb, J.M., Nusser, A., & Dekel, A., 1994, ApJ, 420, 44
- Peebles, P.J.E., 1980, The Large-Scale Structure of the Universe, Princeton Univ. Press, Princeton
- Protogeros, Z.A.M., Melott, A.L., & Scherrer, R.J., 1997, MNRAS, 290, 367
- Protogeros, Z.A.M., & Scherrer, R.J. 1997, MNRAS, 284, 425 (PS)
- Scoccimarro, R., Couchman, H., & Frieman, J.A., 1999, ApJ, 517, 531
- Watts, P.I.R., & Taylor, A.N., 2000, astro-ph/0006192